

TABLE OF CONTENTS

	Page
ACKNOWLEDGEMENTS	iii
ABSTRACT (ENGLISH)	v
ABSTRACT (THAI)	viii
LIST OF TABLES	xx
LIST OF FIGURES	xxi
ABBREVIATIONS AND SYMBOLS	xxxii
CHAPTER 1 INTRODUCTION	
1.1 Zinc oxide	3
1.1.1 Crystal structure	3
1.1.2 Mechanical properties	5
1.1.3 Electronic properties	5
1.1.4 Optical properties	6
1.1.5 Applications	8
1.1.6 Doping ZnO with a metal	8
1.1.7 ZnO nanostructure	9
1.2 Niobium	10
1.3 Flame Spray Pyrolysis (FSP)	13

1.3.1	The basic steps of particle formation and growth by gas-to-particle conversion in FSP	17
1.3.1.1	Nucleation	17
1.3.1.2	Nucleated condensation	17
1.3.1.3	Coagulation	18
1.3.1.4	Coalescence	20
1.4	The theory of characterization techniques	22
1.4.1	X-ray diffraction method	22
1.4.1.1	Crystal structure	22
1.4.1.2	Bragg's Law	24
1.4.1.3	Crystallinity	25
1.4.1.4	Lattice parameters	26
1.4.1.5	Powder diffraction and identification of phases by XRD	26
1.4.2	Brunauer-Emmett-Teller (BET) analysis-Particle size (d_{BET})	28
1.4.3	Scanning Electron Microscope (SEM)	29
1.4.4	Energy Dispersive X-ray Spectroscopy (EDS)	33
1.4.5	Transmission Electron Microscopy and diffraction	34
1.4.6	UV-Vis absorption spectroscopy	37
1.4.6.1	Beer's Law	39
1.4.6.2	Tauc's relation	39
1.4.7	Atomic Force Microscopy (AFM)	43

1.4.7.1 Basic principles	44
1.4.7.2 Imaging modes	45
1.4.7.3 AFM cantilever deflection measurement	48

REFERENCES

49

CHAPTER 2 SYNTHESIS AND CHARACTERIZATION

OF PURE ZnO AND Nb-DOPED ZnO NANOPARTICLES

2.1	Research overviews	60
2.1.1	Synthesis of ZnO nanoparticles	60
2.1.2	Flame spray synthesis of nanoparticles	62
2.1.3	Flame spray pyrolysis based on pure ZnO and metal-doped ZnO	64
2.2	Experimental	69
2.2.1	Chemicals and equipments	69
2.2.2	Solubility test	69
2.2.3	Precursor preparation for FSP	71
2.2.4	Procedures for synthesizing nanoparticles by FSP	73
2.2.5	Particle characterization method	75
2.3	Results and discussion	76
2.3.1	Nanoparticles synthesis	76
2.3.1.1	Flame-made pure ZnO and Nb-doped ZnO nanoparticles	76
2.3.1.2	Powder appearance	77

2.3.2	Characterization of flame-made nanoparticles	77
2.3.2.1	X-ray diffraction analysis	77
2.3.2.2	BET analysis	79
2.3.2.3	Transmission electron microscopy (TEM) and Energy dispersive x-ray spectroscopy (EDS)	80
2.3.2.4	Scanning Electron Microscopy (SEM) and Energy Dispersive X-ray Spectrometry (EDS): dot-mapping modes	85
2.3.2.5	UV-vis absorption spectroscopy	88
2.4	Conclusions	90
REFERENCES		91

CHAPTER 3 APPLICATION OF PURE ZnO AND Nb-DOPED

ZnO FOR USE AS PHOTOVOLTAIC DEVICES

3.1	Introduction	98
3.1.1	Inorganic solar cells	98
3.1.2	Organic solar cells	99
3.1.3	Advantages of organic solar cells	103
3.1.4	Characterization of organic bulk heterojunction solar cells	103
3.1.5	Principles of bulk heterojunction solar cell	103
3.1.6	Literature review	109
3.2	Chemicals and equipments	116

3.2.1	Solar cell preparation	116
3.2.2	Solar cell characterization	117
3.3	Experimental	118
3.3.1	Device fabrication	118
3.3.1.1	The effect of Nb loading on the solar efficiency of the P3HT:PCBM:Nb-doped ZnO blend films and the amount of Nb-doped ZnO loading on the solar efficiency of the P3HT:PCBM:Nb-doped ZnO blend films	118
3.3.1.2	The effect of niobium doping on composite solar cells using the 3 mol% Nb-doped ZnO NPs and the use of 1,3,5-trichlorobenzene (TCB) as co-solvent for enhancing nanostructured P3HT:PCBM:Nb/ZnO layer	119
3.3.2	Measurements and characterization	120
3.4	Results and Discussion	122
3.4.1	The effect of Nb loading on the solar efficiency of the P3HT:PCBM:Nb-doped ZnO blend films and the amount of Nb-doped ZnO loading on the solar efficiency of the P3HT:PCBM:Nb-doped ZnO blend films	122

3.4.2	The effect of niobium doping on composite solar cells using the 3.00 mol% Nb-doped ZnO nanoparticles and the use of 1, 3, 5- trichlorobenzene (TCB) as co-solvent for enhancing nanostructured P3HT:PCBM: Nb-doped ZnO layer	130
3.5	Conclusions	135
	REFERENCES	136

CHAPTER 4 APPLICATION OF PURE ZnO AND Nb-DOPED ZnO FOR USE AS GAS SENSORS

4.1	Introduction	145
4.1.1	Gas sensing mechanism	149
4.1.2	Temperature Limitations	153
4.1.3	Response and recovery time	154
4.1.4	Selectivity	155
4.1.5	Metal additives affect	155
4.1.6	Literature review	157
4.2	Chemicals and equipments	165
4.3	Experimental	165
4.3.1	Sensing film fabrication	165
4.3.2	Sensing film Characterization	166
4.3.3	Gas sensing characterization	166
4.4	Results and discussion	168

4.4.1	Sensing film properties	168
4.4.1.1	X-ray diffraction analysis	168
4.4.1.2	SEM-film thickness sensing layer	169
4.4.1.3	Energy Dispersive X-ray Spectrometry (EDS): line scan mode	170
4.4.2	Gas sensing properties	175
4.5	Conclusions	185

REFERENCES

186

CHAPTER 5 APPLICATION OF PURE ZnO AND Nb-DOPED ZnO FOR USE AS PHOTOCATALYSTS

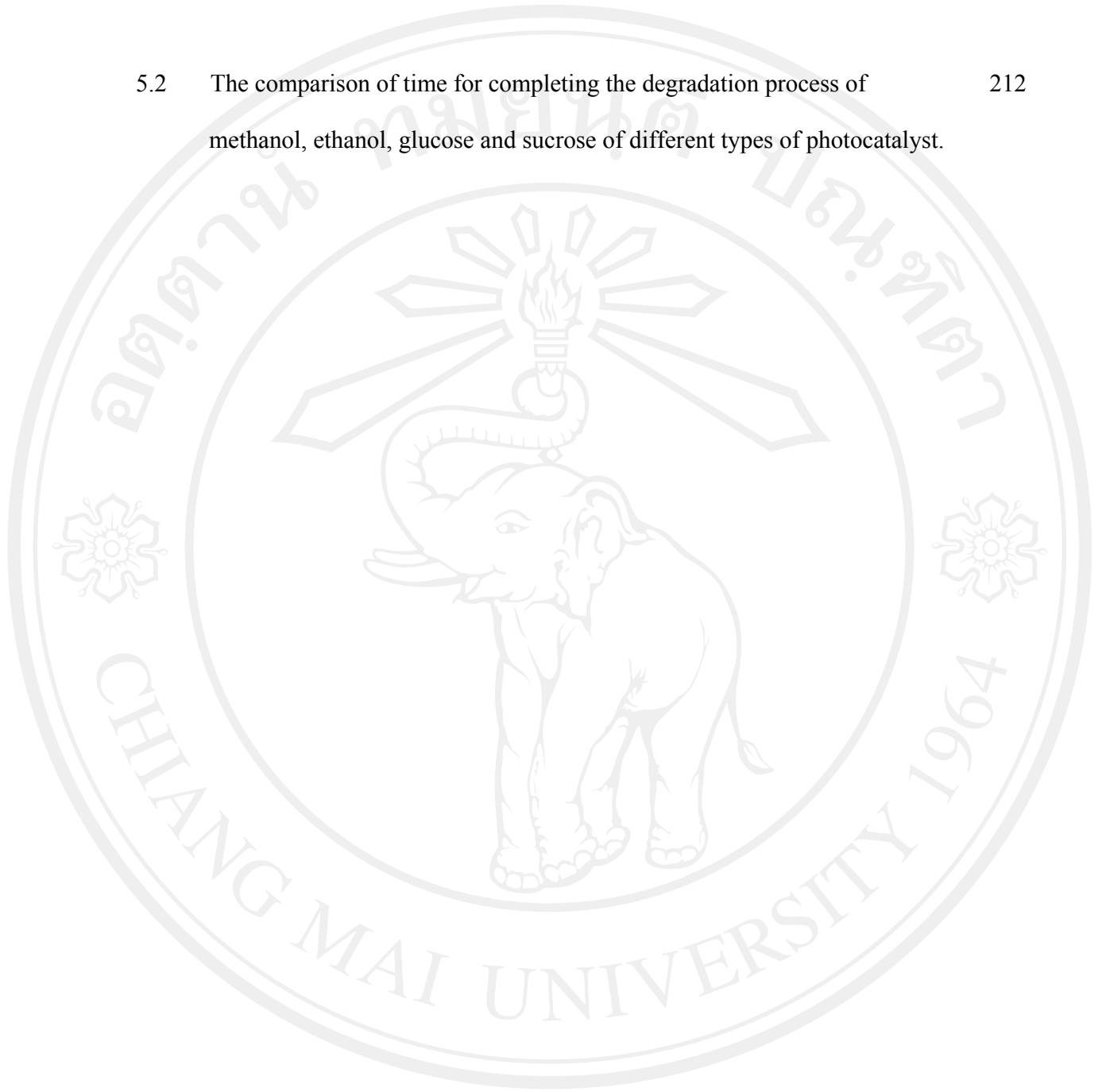
5.1	Introduction	192
5.1.1	Function and principles of photocatalysts	195
5.1.2	Photocatalytic oxidation	197
5.1.3	Photocatalytic reduction	198
5.1.4	Effect of surface area on photocatalytic activity	198
5.1.5	Effect of electron-hole recombination on photo catalytic activity	199
5.1.6	Design of photocatalysts of high activity	200
5.1.7	Increasing efficiency by incorporation of metal nanoparticles	200
5.1.6	Literature review	202
5.2	Chemicals and equipments	206

5.3	Experimental	207
5.3.1	Calibration curve measurement	207
5.3.2	Preparation of photocatalyst suspension and operation	207
5.4	Results and discussion	209
5.5	Conclusions	212
	REFERENCES	214
	CURRICULUM VITAE	222

LIST OF TABLES

Table		Page
1.1	The basic materials parameters of wurtzite ZnO.	7
1.2	The electron configuration of vanadium, niobium and tantalum.	10
1.3	Physical properties of Nb.	13
2.1	Ag-ZnO catalysts prepared via FSP (3/8, 5/5, 8/3) and wet-phase synthesis together with measured SSA and reaction performance in photodegradation of MB.	68
2.2	Precursor preparation for FSP.	72
3.1	Nonexhaustive survey of reports focusing on photovoltaic devices based on P3HT:PCBM and P3HT:PCBM: Metal or Metal Oxide blends.	110
3.2	Solar cell parameters.	125
3.3	Solar cell parameters.	128
3.4	Solar cells characteristics of P3HT: PCBM and P3HT:PCBM:3.00 mol% Nb-doped ZnO bulk-hetero junction solar cells blends (both with and without added TCB) annealed for 5 and 7 min.	132
4.1	A summary on the gas sensing properties of pure/doped metal oxide semiconductors for NO ₂ , CO, C ₂ H ₅ OH and acetone gas.	157
5.1	The common chemical oxidants, placed in the order of their oxidizing Strength.	197

5.2	The comparison of time for completing the degradation process of methanol, ethanol, glucose and sucrose of different types of photocatalyst.	212
-----	--	-----



ลิขสิทธิ์มหาวิทยาลัยเชียงใหม่
Copyright© by Chiang Mai University
All rights reserved

LIST OF FIGURES

Figure		Page
1.1	crystal structure of zinc oxide. (a) Wurtzite phase ZnO, (b) Zincblende phase ZnO.	4
1.2	The periodic table.	11
1.3	Sketch of the basic steps of particle formation.	16
1.4	Steps leading to grain growth by coalescence of small and large grains with a curved grain boundary.	20
1.5	Image of a lab-scale reactor (right). The critical sub-processes in the FSP process and their approximate spatial location are indicated on the left. Nanoparticle samples extracted from the flame at the indicated heights are shown.	21
1.6	A unit cell from a three dimensional lattice.	23
1.7	Deriving Bragg's law using the reflection geometry and applying Trigonometry.	24
1.8	XRD pattern of FeOOH sample.	27
1.9	X-ray diffraction system used in this research.	2
1.10	Schematic diagram of a typical SEM.	31
1.11	Electrons produced in SEM.	32
1.12	SEM system used in this research.	32

1.13	Schematic diagram of a TEM.	36
1.14	TEM system used in this research.	36
1.15	Attenuation of a beam of radiation by an absorbing solution. The larger arrow on the incident beam signifies a higher radiant power than is transmitted by the solution. The path length of the solution is b , and the concentration is c .	38
1.16	Schematic diagram of the absorption process.	40
1.17	UV-vis spectrum of nanostructured zinc oxide.	42
1.18	Varian Cary 50 UV-vis absorption spectrophotometer.	42
1.19	Drawing of basic principle of AFM. A cantilever, with a very small tip (probe), moves along the surface and experiences atomic forces. Laser and Photodiode are used to measure those forces.	43
2.1	The solubility tests of the precursors were performed using zinc naphthenate as a Zn precursor dissolved in several organic solvents prior to the precursor preparation.	70
2.2	The solubility tests of the precursors were performed using niobium (V) ethoxide as a Nb precursor dissolved in several organic solvents prior to the precursor preparation.	70
2.3	The solubility tests of the precursors were performed using zinc naphthenate and niobium (V) ethoxide as Zn and Nb precursors dissolved well in toluene:methanol mixture with ratio of 70:30 vol% prior to the precursor preparation.	71

2.4	The experimental setup for flame-made pure ZnO and Nb-doped ZnO nanoparticles.	73
2.5	Spray flame (0.5 M zinc naphthenate and niobium (V) ethoxide in toluene/methanol: 70/30 vol%).	76
2.6	The flame-made (5/5) pure ZnO and 0.10-3.00 mol% Nb-doped ZnO nanoparticles ordered from the left to right with increasing Nb concentrations.	77
2.7	XRD patterns of the flame-made (5/5) pure ZnO and Nb-doped ZnO nanoparticles with different Nb concentrations.	78
2.8	The specific surface area (SSA_{BET}) and BET-particle diameter (d_{BET}) of the flame-made (5/5) pure ZnO and Nb-doped ZnO nanoparticles with different Nb concentrations.	80
2.9	TEM bright-field image of (a, b) pure ZnO, (c, d) 1.00 mol% Nb-doped ZnO nanoparticles and (e, f) 3.00 mol% Nb-doped ZnO nanoparticles.	81
2.10	TEM bright-field image and EDS mode of 1.00 mol% Nb-doped ZnO.	82
2.11	EDS spectrum (line scan mode) of pure ZnO nanoparticles.	83
2.12	EDS spectrum (line scan mode) of pure 0.25 mol% Nb-doped ZnO nanoparticles.	83
2.13	EDS spectrum (line scan mode) of pure 0.50 mol% Nb-doped ZnO nanoparticles.	84
2.14	EDS spectrum (line scan mode) of pure 1.00 mol% Nb-doped ZnO nanoparticles.	84

2.15	EDS spectrum (line scan mode) of pure 3.00 mol% Nb-doped ZnO nanoparticles.	85
2.16	SEM image and EDS dot-mapping modes of the flame-made (5/5) pure ZnO nanoparticles.	86
2.17	SEM image and EDS dot-mapping modes of the flame-made (5/5) 0.25 mol% Nb-doped ZnO.	86
2.18	SEM image and EDS dot-mapping modes of the flame-made (5/5) 0.50 mol% Nb-doped ZnO.	87
2.19	SEM image and EDS dot-mapping modes of the flame-made (5/5) 1.00 mol% Nb-doped ZnO.	87
2.20	SEM image and EDS dot-mapping modes of the flame-made (5/5) 3.00 mol% Nb-doped ZnO.	88
2.21	UV-vis absorption spectra of pure ZnO and Nb-doped ZnO	
3.1	Chemical structures and abbreviations of some conjugated organic molecules.	101
3.2	Schematic layout of an organic solar cell.	102
3.3	Schematic drawing of the donor and acceptor energy levels.	103
3.4	Typical J-V characteristics of an organic PV cell.	104
3.5	The interface between two different semiconducting polymers (D = donor, A = acceptor) can facilitate either charge transfer by splitting the exciton or energy transfer, where the whole exciton is transferred from the donor to the acceptor.	107

3.6	Device configuration of the polymer solar cells.	118
3.7	The bulk heterojunction photovoltaic devices (a) before and (b) after depositing with LiF and Al electrode.	120
3.8	The solar simulation system.	121
3.9	The EQE simulation system.	122
3.10	Device structure and energy level diagram of the components.	123
3.11	J-V curves under 120 mW/cm^2 white light illumination of Nb-doped ZnO loading with different Nb concentrations on device performance.	124
3.12	EQE spectra of Nb-doped ZnO loading with different Nb concentrations on device performance.	124
3.13	The J-V curves of P3HT:PCBM:Nb-doped ZnO photovoltaic cells measured in the ambient atmosphere with 120 mW/cm^2 white-light irradiation.	126
3.14	EQE spectra of the device fabricated using BHJ films with 3.00 mol% Nb-doped ZnO concentrations of 24, 27, 30, and 33 vol%.	127
3.15	Absorption spectra of P3HT:PCBM:Nb-doped ZnO films at various concentrations of Nb-doped ZnO solution blended into the P3HT:PCBM active layer.	128
3.16	The J-V curves of P3HT:PCBM:1-butanol photovoltaic cells measured in the ambient atmosphere with 120 mW/cm^2 white-light irradiation.	130
3.17	J-V characteristics of P3HT:PCBM and P3HT:PCBM:3.00 mol% Nb-doped ZnO bulk-hetero junction solar cells blends (both with and without added TCB) annealed for 5 and 7 min.	131

3.18	EQE spectra of P3HT:PCBM and P3HT:PCBM:3.00 mol%Nb-doped ZnO bulk-hetero junction solar cells blends (both with and without added TCB) annealed for 7 min.	133
3.19	AFM images of P3HT:PCBM:3.00 mol% Nb-doped ZnO spin-coated from (a) CB and (b) CB+TCB annealed for 7 min.	134
4.1	Schematic drawings of sensor devices (a) sintered block type, (b) thick- or thin-film type.	146
4.2	Typical characteristics of semiconductor gas sensor: (a) response transient; (b) temperature dependence of gas response; (c) dependence of R_g on gas concentration.	147
4.3	The adsorbed molecule can significantly modify the dielectric property at the surface of the semiconductor gas sensor.	150
4.4	Schematic diagrams of the as-pasted ZnO nanoparticles.	153
4.5	The response and recovery time of n-type semiconductor for reducing gas.	154
4.6	Mechanism of sensitization by metal additive.	156
4.7	(a) Photograph of sensor substrate including interdigitated comb-like Pt electrodes and a resistive heater. (b) Zn thin-film sputtered sensor substrate. (c) A schematic illustration for the sonochemical growth of vertically aligned ZnO nanorod arrays on a sensor substrate.	160
4.8	(a) Photograph of sensor substrate including interdigitated comb-like Au electrodes. (b) ZnO thick-film spin coat sensor substrate.	166
4.9	Gas sensor measurement setup.	167

- 4.10 XRD patterns of the flame-made (5/5) pure ZnO and Nb-doped ZnO nanoparticles with different Nb concentrations, and samples of sensing films were spin-coated on Au/Al₂O₃ substrate after annealing and sensing test at 350°C. 169
- 4.11 SEM micrographs of flame-made ZnO thick films as a sensor. 170
- 4.12 The EDS line scan mode of sensor based on flame-made pure ZnO nanoarticles. 171
- 4.13 The EDS line scan mode of sensor based on flame-made 0.25 mol% Nb-doped ZnO nanoarticles. 172
- 4.14 The EDS line scan mode of sensor based on flame-made 0.50 mol% Nb-doped ZnO nanoarticles. 173
- 4.15 The EDS line scan mode of sensor based on flame-made 1.00 mol% Nb-doped ZnO nanoarticles. 174
- 4.16 Dynamic response of pure ZnO and 0.25, 0.50 and 1.00 mol% Nb-doped ZnO gas sensor towards 0.1–4 ppm NO₂ gas square pulses at 250°C. 175
- 4.17 Dynamic response of pure ZnO and 0.25, 0.50 and 1.00 mol% Nb-doped ZnO gas sensor towards 0.1–4 ppm NO₂ gas square pulses at 300°C. 176
- 4.18 Dynamic response of pure ZnO and 0.25, 0.50 and 1.00 mol% Nb-doped ZnO gas sensor towards 0.1–4 ppm NO₂ gas square pulses at 350°C. 176

- 4.19 The response of Nb-doped ZnO gas sensor towards 4 ppm of NO₂ versus the operating temperature. The composition of 0.50 mol% Nb in ZnO thin film shows a maximum response of 1640 at 300°C. 178
- 4.20 Variation of response (left) of NO₂ concentrations (0.1–4 ppm) and variation of response times (right) with change in resistance at 300°C. 179
- 4.21 Dynamic response of pure ZnO and 0.25, 0.50 and 1.00 mol% Nb-doped ZnO gas sensor towards 50–1000 ppm C₂H₅OH gas square pulses at 350°C. 180
- 4.22 Variation of response of C₂H₅OH concentrations (50–1000 ppm) with change in resistance at 350°C. 181
- 4.23 Dynamic response of pure ZnO and 0.25, 0.50 and 1.00 mol% Nb-doped ZnO gas sensor towards 50–1000 ppm acetone gas square pulses at 350°C. 182
- 4.24 Variation of response of acetone concentrations (50–1000 ppm) with change in resistance at 350°C. 182
- 4.25 Dynamic response of pure ZnO and 0.25, 0.50 and 1.00 mol% Nb-doped ZnO gas sensor element from 50–1000 ppm CO gas square pulses at 350°C. 183
- 4.26 Variation of response of CO concentrations (50–1000 ppm) with change in resistance at 350°C. 184

4.27	Variation of response with concentration of NO ₂ (4 ppm), CO, C ₂ H ₅ OH and acetone (1000 ppm) at 350°C for sensor of pure ZnO as compared to 0.25, 0.50 and 1.00 mol% Nb-doped ZnO.	184
5.1	Bandgap energies for some common semiconductor materials at 0 K.	193
5.2	The electromagnetic spectrum.	193
5.3	Schematic representation of the mechanism of photocatalytic activity. On absorption of photon of energy $h\nu$, electrons are excited from valence band (VB) to conduction band (CB). There is a transfer of electron to oxygen molecule to form superoxide ion radical ($\bullet\text{O}^{-2}$) and a transfer of electron from water molecule to VB hole to form hydroxyl radical ($\bullet\text{OH}$).	196
5.4	Incorporation of silver nanoparticles facilitate longer charge separation by trapping photogenerated electrons.	201
5.5	Schematic diagram of spiral photoreactor.	208
5.6	Photocatalytic degradation rate of methanol on pure ZnO and Nb-doped ZnO nanoparticles with different Nb loading.	209
5.7	Photocatalytic degradation rate of ethanol on pure ZnO and Nb-doped ZnO nanoparticles with different Nb loading.	210
5.8	Photocatalytic degradation rate of sucrose on pure ZnO and Nb-doped ZnO nanoparticles with different Nb loading.	210
5.9	Photocatalytic degradation rate of glucose on pure ZnO and Nb-doped ZnO nanoparticles with different Nb loading.	211

ABBREVIATIONS AND SYMBOLS

Å	Angstrom
Au	Gold
Al ₂ O ₃	Alumina
at%	atomic %
C	Amount of carbon
cm	Centimeter
cm ³ /min	Cubic centimeter per minute
CRT	Cathode-Ray Tube
CVD	Chemical Vapor Deposition
°C	Degrees Celsius
d_{hkl}	Interplanar distance between (hkl) planes
d	the lattice planar spacing or thickness
d_{EM}	different primary particle sizes
CB	Conduction Band
CB	Chlorobenzene
d_{BET}	BET-particle diameter
e ⁻	Electron
eV	Electron Volt
E	binding energy
E_0	Energy of ground state
E_b	Binding energy
E_F	Fermi level
E_g	Optical band gap of the semiconductor
E_{CB}	Conduction band energy
E_{VB}	Valence band energy

E_{vac}	Energy of vacuum level
FF	Fill factor
EPMA	Electron probe micro-analysis by X-ray
g/L	grams/liter
h	Hour
h	Plank's constant (6.63×10^{-34} Js), hour
HMDSO	Hexamethyldisiloxane
HOMO	Highest occupied molecular orbital
h ν	Photon energy
h^+	Hole
I_0	Intensity of the incident beam
I	Intensity of the transmittance
J _{sc}	Short circuit current
ITO	Indium-tin oxide
IUPAC	International Union of Pure and Applied Chemistry
JCPDS	Joint Committee Powder Diffraction Standards
K	Kelvin
keV	Kilo electron volt
kV	Kilo-volt
LUMO	Lowest unoccupied molecular orbital
L/min	Liter per minute
M	Mol per liter
mg	Milligram
min	Minute
mL	Milliliter
m ²	Square meter
mS	Millisiemen
n	Order of diffraction

N_a	Avogadro's number (6.02×10^{23})
O_2	Oxygen gas
$\cdot O_2^-$	Superoxide radical
$\cdot OH$	Hydroxyl radical
rpm	Revolution per minute
R_0	Resistance in air
R_g	Resistance when the gas is present
T	Transmittance
T_{rec}	Recovery time
T_{res}	Response time
VB	Valence band
V_{OC}	Open circuit voltage
V_{mI_m}	The maximum deliverable power
V_m	The volume of gas adsorbed at STP per unit mass of adsorbent, when the surface is covered by a unimolecule layer of adsorbate
Z	Atomic number
λ	Wavelength
μg	Microgram (10^{-6} g)
$\mu g C$	Microgram of carbon
μm	Micron (10^{-6} meter)
μ_s	Electron mobility at the surface
$\mu S/cm$	MicroSiemens /square centimeter
ϵ	Absorptivity
ϵ_0	The permittivity of the vacuum
θ	The Bragg angle for the reflection
ν	Frequency
η	Power conversion efficiency